

# A sea-state-dependent control strategy for wave energy converters: power limiting in large wave conditions and energy maximising in moderate wave conditions

Zhijing Liao, Xiaotao Zhang, Judith Apsley, Matteo F. Iacchetti, Peter Stansby, Guang Li

**Abstract**—Conventional control strategies for wave energy converters (WECs) maximise power capture of the WEC by amplifying its responses, but this exacerbates hardware constraint violations not generally taken into account, causing undesirable shutdown of electrical systems in adverse wave conditions. When WECs operate close to power take-off (PTO) capacity, the primary control objective is to limit peak power for hardware protection purposes, enabling longer continuous electricity generation time.

In this paper, we propose a sea-state-dependent control strategy based on model predictive control to maximise the annual energy production of a WEC with a realistic PTO: in small to moderate sea states it adopts a conventional energy-maximising objective function to increase output power, while in higher sea states a speed-limiting objective function may be utilised to enable longer generating time before shutdown becomes necessary. While this control strategy applies to a wide range of WECs, here we carry out the case study on an attenuator WEC called M4, with gearbox transmission and a permanent magnet synchronous generator (PMSG) as its PTO, which is being designed for a 1/4 scale ocean test in Albany, Australia. Simulation results show that compared with a benchmark passive damping controller, a 66% increase in annual energy production can be expected at the targeted site.

**Index Terms**—Wave energy converter, wave-to-wire model, model predictive control, power limiting control

## I. INTRODUCTION

Ocean wave energy represents a promising renewable energy source with an estimated global wave power resource of approximately 2 TW [1]. Wave energy converters (WECs) are devices that harness and convert wave power into electricity. To date, the levelised-cost-of-electricity (LCoE) of wave energy has been too high to make it a competitive energy solution.

Power take-off (PTO) systems of WECs have limited capacity often defined by constraints on the operating torque and speed. Conventional energy-maximising controllers improve power capture by increasing the responses (torque and speed) of the PTO, for example, reactive control [2], latching control

[3], and optimization-based control [4], [5], etc. In large wave conditions, this can lead to constraint violations of the PTO, resulting in a shutdown of the PTO in some sea states for hardware protection purposes. Since shutdown always happens in relatively high sea states, where more power is available, frequent shutdowns can reduce annual energy production significantly.

This issue may be mitigated by selecting PTO components with higher-rated values. However the high capacity requirement of a PTO can substantially increase its hardware cost, and finally a high LCoE. Thus the capacity of a properly designed PTO needs to be fully utilized in most sea states, which will inevitably trigger safety limits at relatively large sea states. Another option with some advanced energy-maximising controllers [4], [5] is to handle the torque or speed constraints using online optimization solvers. However, the energy-maximising control objective is in direct conflict with the power-limiting goal, rendering these constrained optimization problems infeasible for larger sea states. Although this issue can be potentially handled as discussed in [6] to ensure a solution from the optimisation solver, this solution is sub-optimal. The actual challenge, that is the risk of hardware constraint violations, cannot be resolved without the introduction of a new controller.

Motivated by these arguments we propose a sea-state-dependent control strategy to maximise net electricity generation and reduce the shutdown times in high sea states based on model predictive control (MPC) by combining two control algorithms: (a) energy maximising; (b) power limiting. In small to moderate sea states where constraint violations happen infrequently, the MPC adopts an energy-maximising objective function to increase output power. In higher sea states, a speed-limiting objective function may be utilised by the MPC to limit the speed of the PTO providing a longer generating time. This control strategy applies to a wide range of WECs as PTOs share the same power-limiting control problem. Here, we apply the strategy to an attenuator WEC called M4 with an all-electric PTO as a case study to demonstrate the efficacy.

The M4 WEC is a multi-float multi-mode motion WEC which has been studied extensively over the past decade. Hydrodynamic design is optimised by wave basin tests [7], [8] and hydrodynamic control based on linear diffraction modelling and optimal control has been demonstrated [9].

Zhijing Liao (zhijing.liao@manchester.ac.uk), Xiaotao Zhang (xiaotao.zhang@manchester.ac.uk), Judith Apsley (j.apsley@manchester.ac.uk), Matteo F. Iacchetti (matteo.iacchetti@manchester.ac.uk), Peter Stansby (p.k.stansby@manchester.ac.uk) and Guang Li (guang.li@manchester.ac.uk) are with the School of Engineering, University of Manchester, Manchester, M13 9PL, UK.

Matteo F. Iacchetti is also with the Department of Energy, Politecnico di Milano, Milan, Italy.

Efficient mooring design is currently under investigation [10]. The full-scale capacity with multi-PTOs is estimated to be at the same level as offshore wind [11]. To advance development, a 1/4 scale sea trial is being planned for Albany, Western Australia. A mechanical gearbox and a permanent magnet synchronous generator (PMSG) will be used to generate electricity. In this paper, a wave-to-wire (W2W) modelling method is adopted to include coupling dynamics and constraints from both mechanical and electrical components which will be based on those for the ocean trial. The maximum speed of the PMSG is a key constraint of this W2W model. The intention of applying the sea-state-dependent control strategy to this system is to reduce the occurrence of constraint violations, especially in large wave conditions. It will be shown with the proposed strategy, the annual energy production can be significantly improved at the targeted sea trial site with varying sea conditions.

Note that the changeover between different controllers is assumed to be done in a “Cold Boot” way. The PTO will be shut down and rebooted to enter a new control stage dependent on the sea state. This distinguishes the current work from traditional switching control methodologies [12], [13].

The idea of adopting a wind-speed dependent control strategy has found success in the field of variable-speed wind turbine control, as reviewed in e.g. [14]. The control of wave energy converters shares the same challenge but there is a clear gap in knowledge in the literature to tackle this challenge. The novel contribution of this work is thus the introduction of a sea-state-dependent control strategy to the field of wave energy converter control.

The rest of the paper is arranged as follows: Section 2 describes the W2W modelling, focusing mainly on the dynamics of the M4 platform and the PMSG. Section 3 addresses the controller design for the W2W model, including the local field-oriented controller of the PMSG and the upper-level model predictive control for both the energy-maximising stage and the power-limiting stage. Results from numerical simulations and analysis are presented in section 4 while the conclusion is drawn in section 5.

## II. W2W MODELLING

### A. The M4 hydrodynamic model

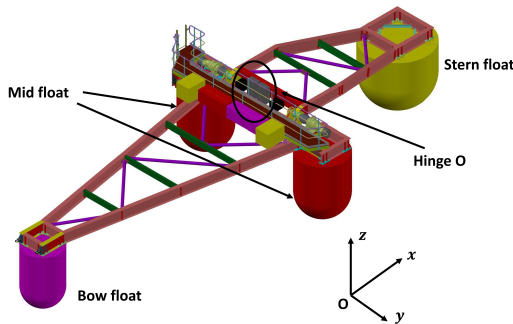


Fig. 1: The M4 1-2-1 design diagram, provided by BMT, Australia.

The quarter-scale version of M4, as shown in Fig. 1, is considered in this work. It is about 21.3 m long and 9.5 m wide. There are, in total, four floats, one bow float connected rigidly with two middle floats and one stern float connected separately on the other side. When moored, from a single point mooring, the platform heads naturally into wave direction due to wave drift forces. As waves propagate through the device, motions of the bow, mid and stern floats are out of phase to varying degrees, which causes the device to rotate about the hinge, with a damper converting the wave power into mechanical power of the device. The PTO is located at the hinge to generate electricity from the rotational motion. Mass and dimension of each float including ballast are shown in Table I.

Part	mass (kg)	h (m)	t (m)	v (m)	radius (m)
float 1	2308	-13.3	0	-2.41	1
ballast 1	1090	-13.3	0	-3.91	
float 2	3100	0	-3.5	-2.34	1.25
ballast 2	1719	0	-3.5	-0.63	
float 3	3100	0	3.5	-2.34	1.25
ballast 3	1719	0	3.5	-0.63	
float 4	4371	8	0	-2.39	1.75
ballast 4	10570	8	0	-3.72	

TABLE I: Centre of mass is relative to hinge  $O$ .  $h$  (horizontal) is for the  $x$ -axis;  $t$  (transversal) is for the  $y$ -axis;  $v$  (vertical) is for the  $z$ -axis. The radius is of the circular cross-section.

Linear diffraction/radiation methods based on potential flow theory have been used to model the dynamics of the platform in operational sea conditions [15]. This is then converted into a control-oriented state-space form by system identification and model order reduction [16] for controller design purposes. The modelling procedure is briefly reported here.

As power is mainly captured by the surge, heave and pitch motions, it is reasonable to only model dynamics in these degrees of freedom (DOFs). The motion vector can be defined as  $\eta = [x_0 \ z_0 \ \theta_l \ \theta_r]^\top$ , where  $x_0$  and  $z_0$  are the surge and heave motion of the reference point at the centre of the hinge,  $\theta_l$  is the relative pitch motion of the bow-mid float frame and  $\theta_r$  is the relative pitch motion of the stern float, both with respect to the reference point.

Based on Newton’s Second Law of Motion, the equation of motion for the M4 WEC in the time domain based on linear waves is

$$M\ddot{\eta}(t) = f_{e,\eta}(t) + f_{rd,\eta}(t) + f_{rs,\eta}(t) + f_{pto,\eta}(t) \quad (1)$$

where  $M$  is the  $4 \times 4$  mass and inertia matrix, including inertia from the gearbox and electrical generator.  $f_{e,\eta}(t)$  is the wave excitation force,  $f_{rd,\eta}(t)$  is the radiation damping force,  $f_{rs,\eta}(t)$  is the hydrostatic restoring force and  $f_{pto,\eta}(t)$  is the PTO torque. Note that the mooring force is not modelled for simplification but a small stiffness term is added to the surge DOF to prevent model drift.

The wave excitation force is independent of the WEC motion. It can be calculated using

$$f_{e,\eta}(t) = Re\left\{\sum_{n=1}^{N_\omega} H(\omega_n) F_{ex,\eta}(\omega_n) e^{i(\omega_n t + \phi(\omega_n))}\right\} \quad (2)$$

where  $H(\omega_n)$  is the complex wave spectrum and  $F_{ex,\eta}(\omega_n)$ , which can be obtained with coefficients from the hydrodynamic solver WAMIT [17], is the excitation force exerted on each DOF in coordinate  $\eta$  by a unit-amplitude monochromatic wave of frequency  $\omega_n$ .  $\phi(\omega_n)$  is the random phase shifts associated with each frequency to differentiate between runs.  $N_\omega$  is the number of total frequencies considered in WAMIT and in this case  $N_\omega = 200$ . Maximum and minimum frequencies in  $\omega_n$  are 0.83 Hz and 0.03 Hz. This equation is used in numerical simulations to generate wave excitation force profiles. Note that  $\omega_n$  can be interpolated with a higher  $N_\omega$  value to avoid the wave profile repeating itself in long runs.

The radiation force in the time domain is modelled in convolution form using Cummins' method [18].

$$f_{rd,\eta}(t) = -\int_{-\infty}^t F_{rd}(t-\tau) \dot{\eta}(\tau) d\tau \quad (3)$$

where  $F_{rd}$  is a  $4 \times 4$  matrix with an impulse response function (IRF) calculated using radiation damping coefficients in each entry. The lower limit  $-\infty$  of the integral can be approximated by a finite time  $t_k = t - 12$  with negligible loss of fidelity. These convolutions are then further approximated by a state-space model. This radiation damping state-space representation can be written as:

$$\begin{aligned} \dot{z}_s &= A_s z_s + B_s \dot{\eta}(t) \\ f_{rd,\eta}(t) &= C_s z_s + D_s \dot{\eta}(t) \end{aligned} \quad (4)$$

where  $z_s$  is the auxiliary state variable of the identified state-space sub-system. The size of the state matrices  $A_s$ ,  $B_s$ ,  $C_s$ ,  $D_s$  can be manually chosen and has a great impact on the order of the final state-space model.

The hydrostatic restoring force can be calculated using

$$f_{rs,\eta}(t) = -K\eta(t) \quad (5)$$

where  $K$  is the  $4 \times 4$  hydrostatic restoring matrix.

Equation (1) can now be rewritten as

$$\begin{aligned} (M + m_\infty) \ddot{\eta}(t) - f_{rd,\eta}(t) - f_{rs,\eta}(t) &= f_{e,\eta}(t) + f_{pto,\eta}(t) \\ \dot{z}_s &= A_s z_s + B_s \dot{\eta}(t) \\ f_{rd,\eta}(t) &= C_s z_s + D_s \dot{\eta}(t) \end{aligned} \quad (6)$$

where  $m_\infty$  is the  $4 \times 4$  added mass matrix.

The PTO torque  $f_{pto,\eta}$  is provided by the PMSG based on the upper-level control algorithm through the gearbox ratio.

$$f_{pto,\eta}(t) = \begin{bmatrix} 0 \\ 0 \\ -T_\eta(t) \\ T_\eta(t) \end{bmatrix} \quad (7)$$

where  $T_\eta = T_e d_{gear}$ ,  $T_e$  is the PTO torque on generator side,  $T_\eta$  on the platform side and  $d_{gear}$  is the gear ratio.

By defining a new state vector  $x := [\eta, \dot{\eta}, z_s]^\top$ , the final linear state-space representation of the M4 WEC can be written as:

$$\begin{aligned} \dot{x} &= A_c x + B_{wc} f_{e,\eta}(t) + B_{uc} f_{pto,\eta}(t) \\ y &= C_c x \end{aligned} \quad (8)$$

where the system matrices are

$$A_c = \begin{bmatrix} 0_{4 \times 4} & I_{4 \times 4} & 0_{4 \times n} \\ -(M+m_\infty)^{-1}K & -(M+m_\infty)^{-1}D_s & -(M+m_\infty)^{-1}C_s \\ 0_{n \times 4} & B_s & A_s \end{bmatrix} \quad (9)$$

$$B_{wc} = \begin{bmatrix} 0_{4 \times 4} \\ (M+m_\infty)^{-1} \\ 0_{n \times 4} \end{bmatrix} \quad (10)$$

$$B_{uc} = \begin{bmatrix} 0_{4 \times 1} \\ (M+m_\infty)^{-1}[0, 0, -1, 1]^\top \\ 0_{n \times 1} \end{bmatrix} \quad (11)$$

$$C_c = [0_{1 \times 4} \quad [0 \ 0 \ 1 \ -1] \quad 0_{1 \times n}] \quad (12)$$

where  $I$  is the identity matrix and  $0$  is the matrix with zeros in all entries. The size of  $A_c$  depends on the selected model order  $n$  for the radiation sub-system. The system output  $y = \omega_\eta$  is the rotational velocity on the platform side.

### B. The PMSG model

The rated power of the PMSG is 6 kW, with a rated speed of 1500 rpm. The current limit has been extended to twice the rated value for a maximum available torque of 76.4 Nm. The full PMSG parameters adopted for this paper are listed in Table II. Readers are referred to [19] for more details of the PTO including how the PMSG rating is selected.

Parameters	Values
Rated power	6 kW
Rated speed	1500 rpm
Maximum speed	3089 rpm
Rated torque	38.2 Nm
Maximum torque	76.4 Nm
Pole pairs	8
Rated voltage	415 VLL
Rated current	10.2 A

TABLE II: PMSG parameters.

The PMSG dynamic model is described using a second-order nonlinear state space model in a synchronous reference frame (dq frame), using motoring and constant power transformation conventions, as follows:

$$\begin{aligned} \frac{di_d}{dt} &= \frac{1}{L_d}(v_d - Ri_d + L_q \omega_e i_q) \\ \frac{di_q}{dt} &= \frac{1}{L_q}(v_q - Ri_q - L_d \omega_e i_d - \psi_m \omega_e) \\ T_e &= p[\psi_m i_q + (L_d - L_q)i_d i_q] \end{aligned} \quad (13)$$

where  $v$  is the voltage,  $i$  is the current,  $T_e$  is the torque,  $\psi_m$  is the magnet flux linking stator coils,  $\omega_e$  is the rotor angular speed given in equivalent electrical value.  $p$  is the pole pairs,  $R$  is the resistance,  $L$  is the inductance. Subscripts  $dq$  give the synchronous axes. The generator model assumes a non-salient surface PM generator with  $L_d = L_q$  and neglects all

saturation, including cross saturation. Copper losses are included, but iron and mechanical losses are excluded. Thermal effects are neglected so the magnet flux linkage, inductance and resistance are treated as constant.

### III. CONTROLLER DESIGN FOR THE W2W MODEL

In this section, the complete control scheme of the M4 W2W system is presented. The ultimate goal of control is to maximise the efficiency of the wave energy conversion system in a wide range of sea conditions given the predefined hardware components. A hierarchical framework is adopted. Firstly, local control algorithms of the PMSG are developed. The interface to an upper-level controller is specified and constraints are analysed. Following that, an upper-level control algorithm is designed, which serves two purposes: maximising energy output at low to medium wave height sea states and limiting the rotational speed of the PMSG at higher sea states.

#### A. The PMSG's local controller design

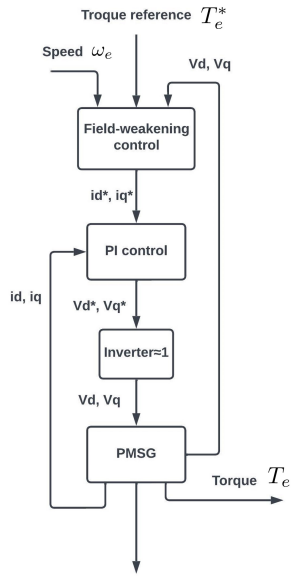


Fig. 2: The block diagram of the local field-oriented controller of the PMSG.

Fig. 2 presents the control flowchart of the local control algorithm of the PMSG. The PMSG is controlled using field-oriented control, based on the measured rotational velocity  $\omega_e$  and the torque reference  $T_e^*$  provided by the upper-level controller.

The field weakening controller takes  $\omega_e$  to work out the current reference  $i_d^*$ , where the controller has been modified to use a pseudo-steady-state analytical method to fit the slow dynamics of the WEC platform controller, see [20] for more details. The current reference  $i_q^*$  is found by (14) with torque limit applied ( $T_e^* \leq T_{lim}$ ).

$$i_q^* = T_e^* / (p\psi_m) \quad (14)$$

Note that the value of  $T_{lim}$  is dependent on  $\omega_e$  in field-weakening. Both  $i_d^*$  and  $i_q^*$  are constrained by :

$$0 \leq \sqrt{(i_d^*)^2 + (i_q^*)^2} \leq I_{max} \quad (15)$$

where  $I_{max}$  is the maximum allowed current for both power converters and PMSG, which has been increased to twice the rated value of the PMSG for higher torque capability.

Then, the current references  $i_d^*$ ,  $i_q^*$  are passed forward to the inner PI current controller to decide the converter output voltage using:

$$\begin{aligned} v_d^* &= k_p(i_d^* - i_d) + k_i \int (i_d^* - i_d) dt - L_q \omega_e i_q^* \\ v_q^* &= k_p(i_q^* - i_q) + k_i \int (i_q^* - i_q) dt + L_d \omega_e i_d^* + \psi_m \omega_e \end{aligned} \quad (16)$$

Voltage references  $v_d^*$ ,  $v_q^*$  are fed to the inverter with losses ignored, to generate supply voltage  $v_d$  and  $v_q$  for PMSG model shown in (13), subject to constraints:

$$0 \leq \sqrt{v_d^2 + v_q^2} = v_{dq} \leq V_{max} \quad (17)$$

where  $V_{max}$  is the maximum allowed switched voltage from the PMSG converter, which is limited by the DC link and hardware configurations. As mentioned, in simulations, the pseudo-steady-state PTO model in a state-space form is used for the computational efficiency, where the converter is represented by averaged power balancing equations [20]. The DC link is held as a constant to supply the required line voltage to the PMSG and space vector modulation is used for power converters [21]. This limit is applied to the field weakening model with a maximum operational speed of  $\omega_{e,max}$ .

When the motor speed  $\omega_e$  increases, the control input voltages  $v_d$ ,  $v_q$  to the PMSG will increase as well. If  $\omega_e$  further increases and  $v_{dq}$  were to exceed the voltage limit  $V_{max}$ , the field-weakening mechanism will be activated: the field-weakening current  $i_d^*$  is introduced to reduce magnetizing flux from the permanent magnet, which further limits terminal voltage while reducing the maximum allowed torque at high speed. The value of  $V_{max}$  is related to hardware limits and PWM switching implementation from power converters on the DC link. Under the constant power convention,  $V_{max} = v_{dc}/\sqrt{3}$  using space vector modulation [21].

Field weakening is a temporary solution for excessive speed. Constraint violation will happen anyway if  $\omega_e$  exceeds a certain value. As mentioned above, the input voltage  $v_d$ ,  $v_q$  are proportional to the angular speed  $\omega_e$ , and so is  $v_{dq}$ . If  $\omega_e$  continues to increase due to a high wave input to the W2W system, there will be a risk that  $v_{dq} > V_{max}$ , causing loss of control and consequent damage to the power converters. In practice, the PMSG local controller will enter a shutdown mode to protect power electronic components when the speed exceeds the maximum allowed speed  $\omega_{e,max}$  which corresponds to the maximum allowed voltage  $V_{max}$ , resulting in zero generated power. Since shutdown always happens in relatively higher sea states, where more power is available, prolonging the generation time in these sea states is beneficial for annual energy production. This can be achieved by the sea-state-dependent control strategy detailed in the next section.

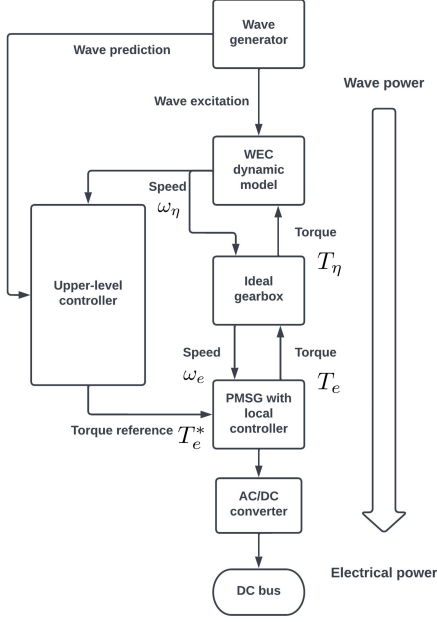


Fig. 3: The control block diagram of the whole W2W model.

### B. Upper-level controller design

Fig. 3 shows the flow chart for the model of the whole WEC system. It comprises six main parts: a wave generator, a WEC dynamic model, an ideal gearbox, a PMSG dynamic model with local torque controllers and an AC/DC converter, a fixed voltage DC bus (enabled by supercapacitor energy storage) and an upper-level energy-maximising controller.

For each simulation, the wave generator pre-calculates the irregular wave excitation forces based on the wave condition  $(H_s, T_p)$  input by the user. It also generates ideal wave excitation forces prediction as an input to the upper-level controller. The WEC dynamic model built based on linear wave theory takes the wave excitation force  $w_k$  and the torque  $u_k = T_{q,k}$  provided by the PMSG through the gearbox as inputs, outputs the rotational velocity  $y_k$  of the WEC platform using the following dynamic equations in a state-space form discretized from (8):

$$x_{k+1} = Ax_k + B_u u_k + B_w w_k \quad (18)$$

$$y_k = \omega_{\eta,k} = Cx_k \quad (19)$$

The upper-level controller utilises the wave prediction information as well as the measured velocity as feedback to generate the optimal torque profile as a reference for the PMSG for maximum power generation. Note that a standard Kalman observer is designed to recover the state information  $x_k$  which is not shown in the flow chart.

The gearbox is assumed to be ideal and it links the speed and torque on the platform side,  $\omega_{\eta}$ ,  $T_{\eta}$  to those on the generator side  $\omega_e$ ,  $T_e$  through the fixed gear ratio. The PMSG generates electrical power by following the output torque reference  $T_e^*$  through the local torque tracking controller which was described in the previous subsection. The generated AC

electrical power is converted to DC power ideally assuming power balance.

1) *Energy-maximising MPC*: In small to moderate amplitude wave conditions where the risk of a shutdown is minor, energy-maximising MPC (em-MPC) is used to generate as much electricity as possible. In this subsection, the formulation of the em-MPC is introduced.

The controller aims to compute a control input sequence over a pre-defined control horizon  $N$  which minimises the objective function:

$$\min_{U_0^N} \sum_{k=0}^N (y_k u_k + R u_k^2 + Q y_k^2) \quad (20)$$

where  $k$  is the discrete time step. The control input  $u_k$  and output  $y_k$  satisfy the discrete-time state-space representation of the WEC dynamic shown in (18) and (19). In (20) the term  $y_k u_k$  represents maximising power since the instantaneous power  $P_k = -y_k u_k$ . The other two terms are used to penalise the control input and output as well as convexifying the optimization problem through the tuning of  $Q$  and  $R$ .

Equation (20) can be converted into a standard quadratic programming (QP) problem [22] subject to constraints representing the limits from the PTO, and then be resolved online by QP solvers (in this paper we use the MATLAB *quadprog* routine) and the first control input from the QP solution is applied following a receding horizon manner.

As mentioned before, for a PMSG, the constraints on torque are dependent on the speed when operating in field weakening. These are taken care of by the local PMSG controller.

2) *Speed-limiting MPC*: As discussed above, the control objective changes from maximising energy to limiting speed in higher amplitude wave conditions. If the em-MPC is still used in these wave conditions, the QP problem may become infeasible. In this section, a speed-limiting MPC (sl-MPC) is proposed. A different objective function is adopted:

$$\min_{U_0^N} \sum_{k=0}^N (R u_k^2 + Q y_k^2) \quad (21)$$

by removing the energy-maximising term  $y_k u_k$ . Equation (21) can also be formulated as a QP problem. Note that this speed-limiting objective function can also be tackled by a conventional linear quadratic regulator (LQR) approach. However, the torque and speed limits of the PTO cannot be optimally handled by the LQR approach, which can lead to potentially worse performance compared with the MPC approach adopted here. For the sl-MPC, constraints on torque and speed of the PMSG are handled in the same way as the em-MPC.

### C. Consideration on wave prediction

Wave prediction is required in this control framework for two purposes:

- Wave excitation force prediction is required for the energy-maximising or speed-limiting MPC. The deterministic sea wave prediction (DSWP) algorithm has shown great potential for this type of control problem and tank testing validation has been demonstrated in [23]



for unidirectional waves. The auto-regressive model that does not require external wave measurements is validated numerically in [24], which serves as an alternative. In this paper, control efficacy is demonstrated assuming ideal prediction accuracy as the main focus is not on wave prediction.

- There are now three different stages of operation: energy maximising, power limiting and shutting down, as shown in Fig. 4. Sea state prediction is needed for the upper-level controller to decide when to switch from one stage to another. In practice, this can be predicted accurately for hours but only prediction for several minutes is needed here. The information about the identified sea state will then trigger the switch based on a predefined look-up table. The PTO will then be completely shut down and attempt to switch to a safer controller after a certain time. In this paper, the changeover between different controllers is assumed to be accomplished automatically. The prime interest is to investigate the performance of the W2W system in a wide range of sea conditions individually and demonstrate the benefit on annual generated energy with the proposed sea-state-dependent control strategy.

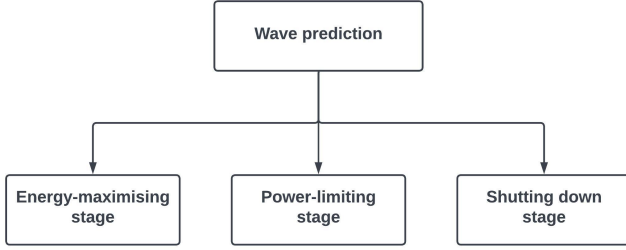


Fig. 4: Switching among different control stages based on wave prediction.

#### IV. SIMULATION RESULTS

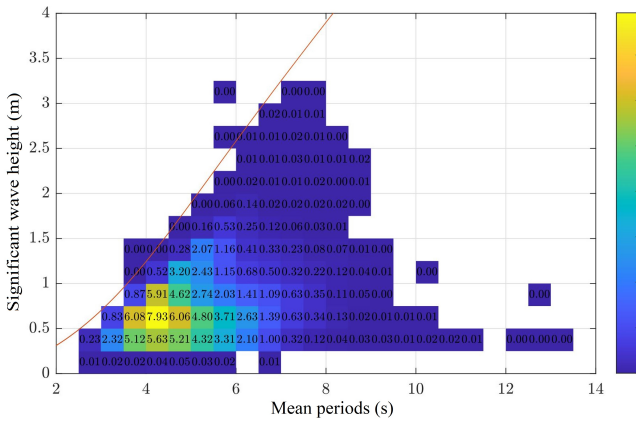


Fig. 5: Scatter diagram [25] of the wave climate at the considered site. Each block represents a specific sea state in which its occurrence rate is shown as a percentage.

$T_p(s)/H_s(m)$	0.5	0.75	1	1.25	1.5
3.5	2.32	0.83	0	0	0
4.2	5.12	6.08	0.87	0	0
4.9	5.63	7.93	5.91	0.52	0
5.6	5.21	6.06	4.62	3.2	0.28
6.3	4.32	4.8	2.74	2.43	2.07
7	3.31	3.71	2.03	1.15	1.16
7.7	2.1	2.63	1.41	0.68	0.41
8.4	1	1.39	1.09	0.5	0.33
9.1	0.32	0.63	0.63	0.32	0.23

TABLE III: Wave conditions and occurrence rate in percentage (%).

Fig. 5 shows a scatter diagram of concerned wave conditions measured at Albany, Western Australia in summer (Nov-March), where the ocean test of the WEC system is being planned. For demonstration purposes, only sea states with significant wave height ( $H_s$ ) from 0.5 m to 1.5 m and peak periods ( $T_p$ ) from 3.5 s to 9.1 s are considered, which cover wave conditions for 96% of the time. Note that peak periods  $T_p$  are assumed to be 1.2 times the mean periods shown in the horizontal axis in Fig. 5. Table III summarises these sea states' occurrence as a percentage. The JONSWAP wave spectrum with a peak enhancement factor of  $\gamma = 3.3$  is used to generate uni-directional irregular wave profiles of these conditions. For each sea state, the run time is 3600 s for estimating the mean generated electrical power and capturing the max rotational speed. The instantaneous electrical power is calculated as

$$P_{ele,k} = -(v_{d,k}i_{d,k} + v_{q,k}i_{q,k}) \quad (22)$$

following motoring conversion and the mean generated power for one sea state is

$$P_{ele} = \frac{T_s \sum P_{ele,k}}{3600 \text{ s}} \quad (23)$$

The sampling rate for simulation is  $T_s = 0.1$  s. The prediction horizon for both energy-maximising and speed-limiting MPCs is  $N = 2T_p$ .

The maximum allowed speed ( $\omega_{e,max}$ ) of the PMSG is 3089 rpm. With a gear ratio  $d_{gear} = 739$ , this means the maximum allowed pitch velocity of the M4 platform is around 4.2 rpm. A speed violation is counted when the measured rotational speed magnitude of the PMSG exceeds the speed limit once in either direction. A sea state is assumed "lost" and has zero generated power if the speed violation occurs more than 10 times per hour. This assumption is made based on the fixed lifetime of mechanical relays that handle the protection in a practical PTO system, provided that annual maintenance can be carried out to replace these components in the WEC system offshore.

##### A. Passive damping control - sea-state-independent

The simple passive damping control method with a sea-state-independent damping ratio is used as a benchmark for comparison as it is easy to implement in practice. For this method, the output torque of the PMSG is negatively proportional to the rotational speed,  $u_k = -d_{pto}y_k$ . A line search

is performed to find the value of  $d_{pto}$  for maximum weighted mean power taking into account the occurrence rate of each sea state. For a sea state  $i$  denote the mean electrical power over the 3600s duration  $P_{ele,i}$  and the occurrence rate of the sea state  $\mathbb{P}_i$ , the annual mean power  $P_{annual}$  is calculated as:

$$P_{annual} = \sum_{i=1}^{N_s} P_{ele,i} \mathbb{P}_i \quad (24)$$

where  $N_s = 45$  is the number of the total sea states.

Fig.6 shows the line search results. The optimum value of  $d_{pto}$  is  $d_{pto} = 379.473 kNm \cdot s/rad$  which gives maximum annual power. One can also notice that larger values of  $d_{pto}$  increase power loss from mechanical to electrical. This is due to higher torque requiring higher current, resulting in a bigger copper loss.

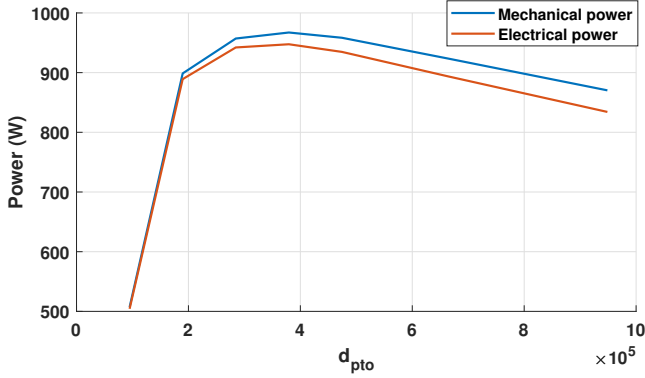


Fig. 6: Annual mean power against  $d_{pto}$ .

$T_p(s)/H_s(m)$	0.5	0.75	1.0	1.25	1.5
3.5	0	255	764	1177	1441
4.2	0	37	199	630	909
4.9	0	0	31	199	529
5.6	0	0	1	38	157
6.3	0	0	0	1	26
7.0	0	0	0	0	3
7.7	0	0	0	0	0
8.4	0	0	0	0	0
9.1	0	0	0	0	0

TABLE IV: Speed violations occurred times in the one-hour simulation for each sea state.

$T_p(s)/H_s(m)$	0.5	0.75	1.0	1.25	1.5
3.5	2148	0	0	0	0
4.2	1514	0	0	0	0
4.9	964	2162	0	0	0
5.6	628	1412	2496	0	0
6.3	424	954	1693	2619	0
7.0	295	663	1179	1836	2617
7.7	210	472	839	1310	1881
8.4	153	343	610	953	1372
9.1	113	255	453	708	1019

TABLE V: Mean electrical power (W) with sea-state-independent passive damping control.

Table IV shows the occurrence of speed violations during the one-hour simulation for each sea state. Underlined values indicate that shutdown happens too frequently in that sea state (over 10 times per hour). As a result, these sea states are assumed lost and the mean electrical power will be set to zero. Readers may also observe that in larger wave periods the occurrence of speed violations is less. This is expected since the WEC has a resonant peak period at  $T_p = 3.5$  s. As  $T_p$  increases, generated power decreases, as does the occurrence of speed violations. Table V summarises the breakdown of mean electrical power in each sea state. The annual mean power with passive damping control is  $P_{annual} = 947$  W.

### B. Passive damping control - sea-state-dependent

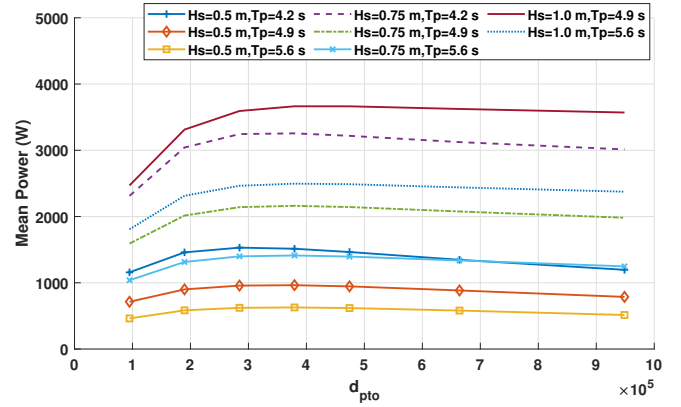


Fig. 7: Mean electrical power against damper ratio  $d_{pto}$  for the eight most frequent sea states.

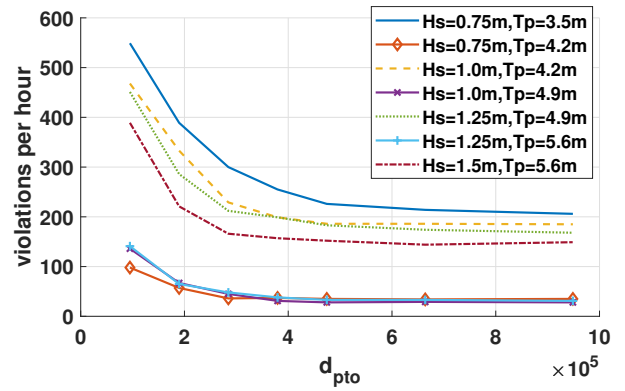


Fig. 8: Over-speed occurrence against different  $d_{pto}$  values in the most relevant sea states.

When sea state prediction is available, it is possible to vary the pre-tuned damping ratio  $d_{pto}$  for different sea states. In this section, the result of passive damping control with sea-state-dependent  $d_{pto}$  is presented as a second benchmark comparison. Fig. 7 shows how the mean electrical power changes with different values of  $d_{pto}$ , for the most frequently occurring sea states. It can be observed that switching between optimal values of  $d_{pto}$  in different sea states does not provide much benefit for the mean electrical power. Fig. 8 shows how

different values of  $d_{pto}$  can affect the occurrence of speed violations. For the sea states where speed violations happen the most, it can be observed that increasing the damping ratio from the optimum value  $d_{pto} = 379.473 \text{ kNm} \cdot \text{s/rad}$  has negligible influences on the number of speed violations. This is due to the fixed capacity (torque limit) of the PTO. Although the optimal values of  $d_{pto}$  are slightly different for some sea states, for passive damping control, switching on the damping ratio  $d_{pto}$  does not improve the overall performance of the WEC system. The annual mean power for passive damping control with switching is  $P_{\text{annual}} = 975 \text{ W}$ .

### C. Energy-maximising MPC - sea-state-independent

In this section, the result with only em-MPC for all the sea states is presented. Figs. 9 and 10 show the responses of the PMSG of one specific sea state,  $H_s = 0.5 \text{ m}$ ,  $T_p = 4.9 \text{ s}$ . Only responses of the first 200 seconds are shown for the sake of clarity. In Fig. 9, the horizontal black dash lines stand for the upper and lower limit of the torque and speed. The em-MPC utilises the wave prediction information to improve power, by making the best use of the allowed torque range and increasing the rotational speed. In Fig. 10, negative power can be observed and the improvement of mean power against passive damping control in this sea state is 63%.

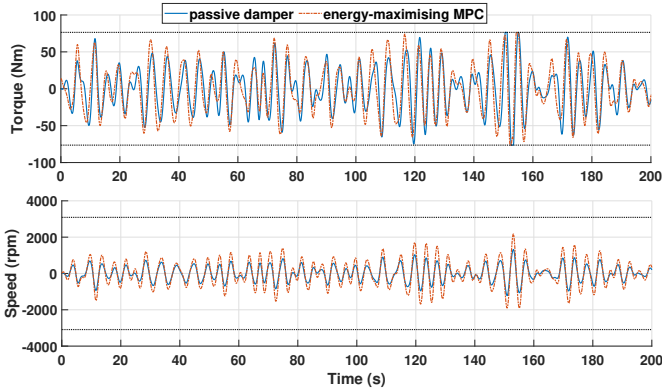


Fig. 9: Time variation of torque and speed comparing the em-MPC and passive damping control.  $H_s = 0.5 \text{ m}$  and  $T_p = 4.9 \text{ s}$ .

Fig. 11 shows the response of the PTO in the torque-speed diagram. The speed  $\omega_{e,k}$  and torque  $T_{e,k}$  at each time step is now a point in the X-Y coordinate. Black thick curves define the allowed operation area of the PMSG with local field weakening controller. Blue scatters represent the response of passive damping control and orange scatters represent that of em-MPC. For both controllers, constraints are well-handled by the PMSG local controller as all scatter dots are within the torque-speed limit curves. The scatter dots of the passive damping control is a straight line in the second and fourth quadrant crossing the origin, since speed and torque are negatively proportional and there is no reactive power for passive damping control. For em-MPC, the scatter dots are distributed in all four quadrants, meaning the PMSG operates in both motoring and generating modes. The maximum speed

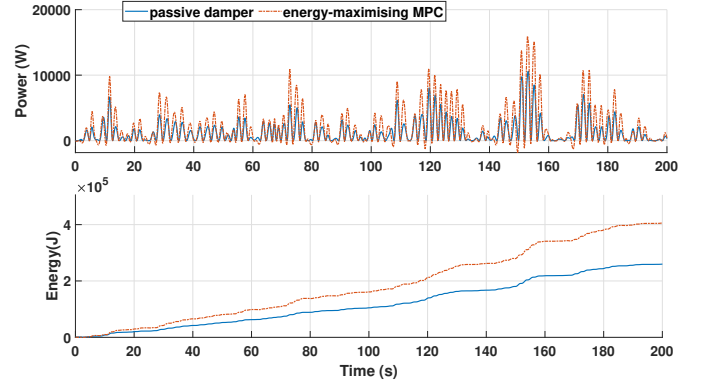


Fig. 10: Time variation of generated electrical power and energy comparing the em-MPC and passive damping control.  $H_s = 0.5 \text{ m}$  and  $T_p = 4.9 \text{ s}$ .

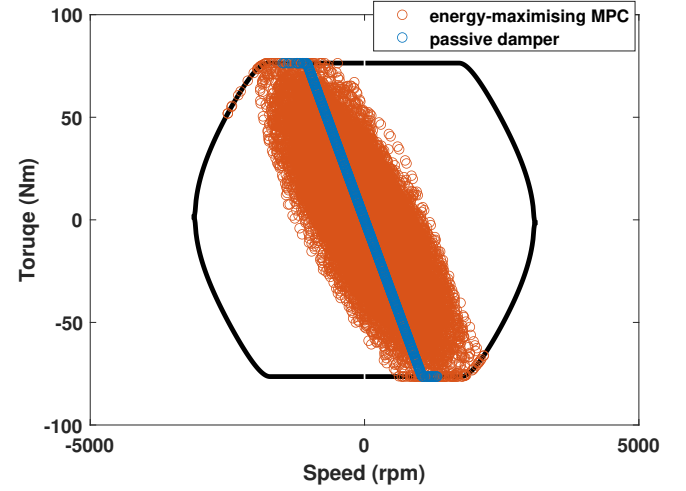


Fig. 11: Trajectory of operation on the torque-speed diagram of the PMSG, comparing the em-MPC and passive damping control.  $H_s = 0.5 \text{ m}$  and  $T_p = 4.9 \text{ s}$ .

is larger than that of passive damping control but still within the allowed range.

Energy-maximising MPC increases power by increasing the response of the PTO. In small sea states, this contributes significantly to the annual mean power. The improvement of mean power over passive damping control is summarised in Table VI as a percentage in each sea state. However, in larger sea states this leads to more frequent speed violations. It can be noticed that for the sea states  $H_s = 0.5 \text{ m}$ ,  $T_p = 3.5 \text{ s}$ ,  $H_s = 1.25 \text{ m}$ ,  $T_p = 6.3 \text{ s}$ , and  $H_s = 1.5 \text{ m}$ ,  $T_p = 7.0 \text{ s}$ , where MPC leads to shutdown of the PTO but passive damping control does not, it is beneficial to switch back to the passive damping control for continuous power generation. This will be discussed in the next section. The annual mean power with the sea-state-independent em-MPC is  $P_{\text{annual}} = 1216 \text{ W}$ , increased by 28% compared with the sea-state-independent passive damping controller.



$T_p(s)/H_s(m)$	0.5	0.75	1.0	1.25	1.5
3.5	2148 <i>damper</i>	0	0	0	0
4.2	2374 (57%)	1331 <i>slmpc</i>	0	0	0
4.9	1574 (63%)	3061 (42%)	1323 <i>slmpc</i>	0	0
5.6	1032 (64%)	2230 (58%)	3360 (35%)	945 <i>slmpc</i>	943 <i>slmpc</i>
6.3	697 (64%)	1548 (62%)	2575 (52%)	2619 <i>damper</i>	1089 <i>slmpc</i>
7.0	484 (64%)	1086 (64%)	1885 (60%)	2732 (49%)	2617 <i>damper</i>
7.7	344 (64%)	774 (64%)	1367 (63%)	2217 (69%)	2780 (48%)
8.4	251 (64%)	564 (64%)	1001 (64%)	1548 (62%)	2162 (58%)
9.1	186 (65%)	419 (64%)	744 (64%)	1159 (64%)	1648 (62%)

TABLE VI: Mean electrical power (W) and improvement over passive damper (%) with em-MPC. In other sea states, the following abbreviations are used in the table: *damper* for switching back to passive damping control, *slmpc* for switching to sl-MPC.

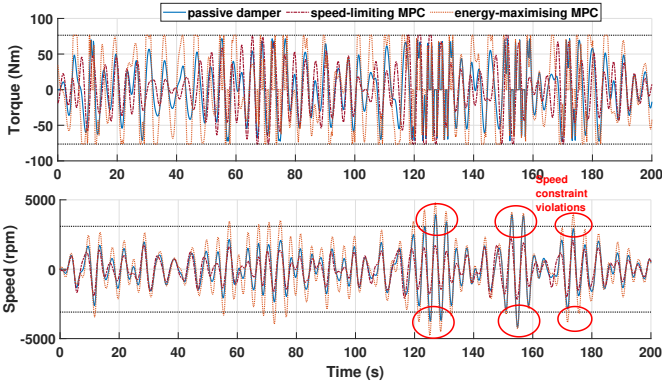


Fig. 12: Time variation of torque and speed comparing the sl-MPC and passive damping control.  $H_s = 1.25$  m and  $T_p = 5.6$  s.

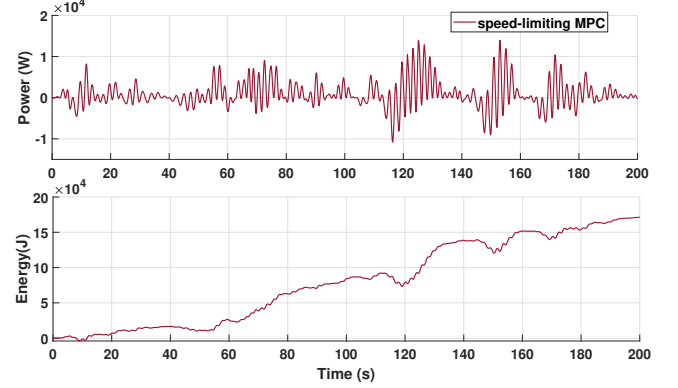


Fig. 14: Time variation of generated electrical power and energy with the sl-MPC.  $H_s = 1.25$  m and  $T_p = 5.6$  s.

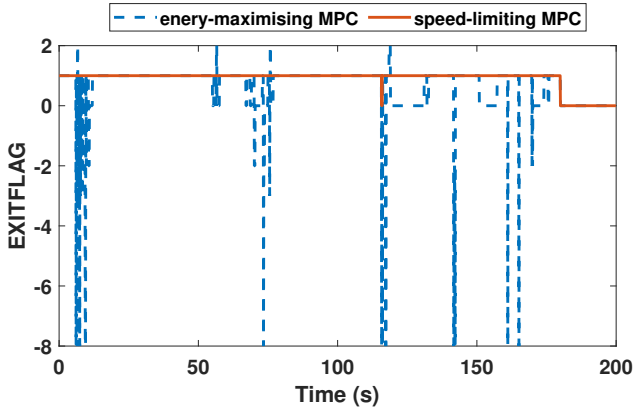


Fig. 13: Feasibility of the QP problem at each sampling interval, comparing two different MPC approaches, observed through the “exitflag” variable returned by the “quadprog” routine. “EXITFLAG=1” means the QP converges to a solution.  $H_s = 1.25$  m and  $T_p = 5.6$  s.

#### D. Speed-limiting MPC and sea-state-dependent control

Speed-limiting MPC can be used to reduce the maximum speed of the PMSG and thus potentially prevent the PTO from shutting down. An example of this is for the sea state with  $H_s = 1.25$  m,  $T_p = 5.6$  s. In this sea state, both the passive damping control and the em-MPC will lead to frequent

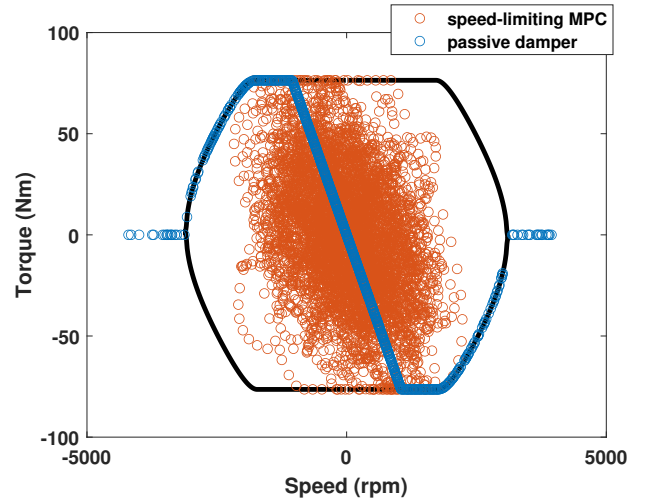


Fig. 15: Trajectory of operation on the torque-speed diagram of the PMSG, comparing the sl-MPC and passive damping control.  $H_s = 1.25$  m and  $T_p = 5.6$  s.

speed violations. Fig. 12 shows the response with the sl-MPC, compared with the other two controllers in this sea state. It can be observed that for both passive damping control and conventional em-MPC, multiple speed violations happen at nearly 120 and 160 seconds. Speed violation happens more frequently for the latter, as expected. For sl-MPC, the speed

response is with smaller amplitudes and speed violation does not happen. Fig. 13 shows the “exitflag” variable returned by the QP solver at each time interval. It can be observed more clearly that in this extreme sea state, the conventional em-MPC has severe infeasibility issues, while the sl-MPC almost always converges to a feasible solution.

Fig. 14 shows the power and energy response of the sl-MPC. Although negative power is more significant compared to em-MPC, the net power is positive. This is extra power provided by the sl-MPC as the PTO would have been shut down in this sea state without it. For this specific PTO, the increased reactive power can be safely handled as the voltage and current constraints on the generator side converter are the same for positive and negative power flow.

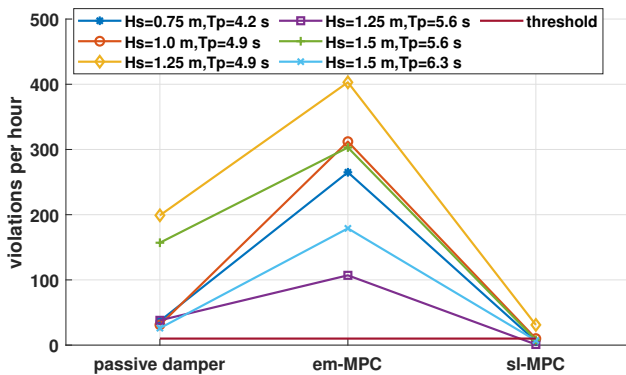


Fig. 16: Speed constraint violations per hour with different controllers.

Fig. 15 shows the trajectory of the sl-MPC compared with the passive damping control. It can be observed more clearly that, with sl-MPC, the PMSG operates within a narrower speed region while with passive damping control, the speed is unbounded. One could also point out the presence of more points close to the field-weakening speed/torque limit curve compared with the energy maximisation method as shown in Fig. 11.

Fig. 16 shows a comparison of occurred speed constraint violations counted within one hour, with the three different controllers in the most concerned sea states. It can be observed that the em-MPC inevitably increases the risk of a shutdown of the PTO, while the sl-MPC can effectively reduce the total violations to below the threshold, demonstrating its efficacy in limiting the speed of the PTO system. Note that although the sl-MPC is effective in reducing the occurrence of speed constraint violations, it makes it difficult for the PTO to generate power at full capacity, as part of the generated power is used to restrain the speed. Hence, it should only be used at high sea states where constraint violations frequently occur. In moderate sea states, em-MPC is preferred.

The overall performance of using the sea-state-dependent MPC is shown in Table VI. The criteria for selecting the controllers for each sea state is: for whichever sea state, prioritise the controller that allows the PTO to avoid constraint violations and shutting down. If both controllers are free from constraint violations, prioritise the one that generates more

power. The annual mean power with the sea-state-dependent MPC is  $P_{annual} = 1575$  W, increased by 66% compared with the benchmark passive damping controller.

## V. CONCLUSION

A sea-state-dependent control strategy is proposed to deal with the control problem of WECs based on their W2W models: energy-maximising in small to moderate sea conditions and power-limiting in larger sea conditions. This is applied as a case study to the W2W model of the quarter scale M4 WEC assumed to be equipped with a gearbox and a 6 kW rated PMSG.

Numerical simulations have been conducted to evaluate the performance of the proposed control scheme, using sea conditions recorded from a sea trial site in Albany, Australia. The results demonstrate a significant improvement in the annual generated electrical power, achieving a 66% increase compared to passive damping control. Notably, without the incorporation of power-limiting control, the improvement is limited to only 28% due to reduced generating time resulting from PTO shutdown.

In the planned ocean test, two gearbox/generator PTOs will be used with a combined torque of 152.8 Nm and power of 10.4 kW to generate power, since sea-state-dependent control is not being applied. Modelling has shown that the annual mean power with two PTOs without sea-state-dependent control is close to the power from one PTO with sea-state-dependent control shown in this paper. Hence, the proposed control strategy effectively reduces the peak-to-mean power ratio by a factor of two.

We should also remark that the improvements of MPC are based on an ideal prediction of the future sea state and incoming wave excitation, although it has been demonstrated that the controllers are reliably robust against prediction error [26]. Besides, only copper loss of the PTO is considered at this stage. Future work should consider incorporating iron loss and mechanical loss of the PTO, which will impact the values of improvement. However, the underlying principle of utilizing a sea-state-dependent control framework, designed based on a W2W model, to optimize the annual power generation of WEC remains valid and similar principles apply to other forms of WEC PTOs.

## ACKNOWLEDGMENT

The authors would like to acknowledge the funding from the Engineering and Physical Sciences Research Council (EPSRC) with grant number EPV0405101.

The M4 WEC was designed in the Blue Economy CRC Project Plan P.3.21.004: Seeding marine innovation in SW WA with a WEC deployment in Albany, funded by the Government of Western Australia, Blue-Economy Cooperative Research Centre, and The University of Western Australia. Fig. 1 is kindly provided by BMT, Australia.

## REFERENCES

- [1] K. Gunn and C. Stock-Williams, “Quantifying the global wave power resource,” *Renewable Energy*, vol. 44, pp. 296–304, 2012. [Online]. Available: <https://www.sciencedirect.com/science/article/pii/S0960148112001310>

- [2] P. Nebel, "Maximizing the efficiency of wave-energy plant using complex-conjugate control," *Proceedings of the Institution of Mechanical Engineers, Part I: Journal of Systems and Control Engineering*, vol. 206, no. 4, pp. 225–236, 1992. [Online]. Available: [https://doi.org/10.1243/PIME\\_PROC\\_1992\\_206\\_338\\_02](https://doi.org/10.1243/PIME_PROC_1992_206_338_02)
- [3] K. Budal and J. Falnes, "Interacting point absorbers with controller motion," *Power from Sea waves*, 1980.
- [4] G. Li and M. Belmont, "Model predictive control of sea wave energy converters – part i: A convex approach for the case of a single device," *Renewable Energy*, vol. 69, pp. 453 – 463, 09 2014.
- [5] R. Genest and J. V. Ringwood, "Receding horizon pseudospectral control for energy maximization with application to wave energy devices," *IEEE Transactions on Control Systems Technology*, vol. 25, no. 1, pp. 29–38, 2017.
- [6] T. K. Brekken, "On model predictive control for a point absorber wave energy converter," in *2011 IEEE Trondheim PowerTech*, 2011, pp. 1–8.
- [7] P. Stansby, E. Carpintero Moreno, T. Stallard, and A. Maggi, "Three-float broad-band resonant line absorber with surge for wave energy conversion," *Renewable Energy*, vol. 78, pp. 132 – 140, 2015. [Online]. Available: <http://www.sciencedirect.com/science/article/pii/S0960148114008957>
- [8] P. Stansby, E. Carpintero Moreno, and T. Stallard, "Capture width of the three-float multi-mode multi-resonance broadband wave energy line absorber m4 from laboratory studies with irregular waves of different spectral shape and directional spread," *Journal of Ocean Engineering and Marine Energy*, vol. 1, no. 3, pp. 287–298, Aug 2015. [Online]. Available: <https://doi.org/10.1007/s40722-015-0022-6>
- [9] Z. Liao, N. Gai, P. Stansby, and G. Li, "Linear non-causal optimal control of an attenuator type wave energy converter m4," *IEEE Transactions on Sustainable Energy*, pp. 1–1, 2019.
- [10] P. Stansby, S. Draycott, G. Li, C. Zhao, E. Carpintero Moreno, A. Pillai, and L. Johanning, "Experimental study of mooring forces on the multi-float wec m4 in large waves with buoy and elastic cables," *Ocean Engineering*, vol. 266, p. 113049, 2022. [Online]. Available: <https://www.sciencedirect.com/science/article/pii/S0029801822023320>
- [11] Z. Liao, P. Stansby, G. Li, and E. C. Moreno, "High-capacity wave energy conversion by multi-float, multi-pt0, control and prediction: Generalized state-space modelling with linear optimal control and arbitrary headings," *IEEE Transactions on Sustainable Energy*, vol. 12, no. 4, pp. 2123–2131, 2021.
- [12] D. Liberzon and A. Morse, "Basic problems in stability and design of switched systems," *IEEE Control Systems Magazine*, vol. 19, no. 5, pp. 59–70, 1999.
- [13] J. Hespanha and A. Morse, "Stability of switched systems with average dwell-time," in *Proceedings of the 38th IEEE Conference on Decision and Control (Cat. No.99CH36304)*, vol. 3, 1999, pp. 2655–2660 vol.3.
- [14] J. G. Njiri and D. Söffker, "State-of-the-art in wind turbine control: Trends and challenges," *Renewable and Sustainable Energy Reviews*, vol. 60, pp. 377–393, 2016. [Online]. Available: <https://www.sciencedirect.com/science/article/pii/S1364032116001404>
- [15] P. Stansby, E. Carpintero Moreno, and T. Stallard, "Large capacity multi-float configurations for the wave energy converter m4 using a time-domain linear diffraction model," *Applied Ocean Research*, vol. 68, pp. 53 – 64, 2017. [Online]. Available: <http://www.sciencedirect.com/science/article/pii/S0141118717302146>
- [16] Z. Liao, N. Gai, P. Stansby, and G. Li, "Control-oriented modelling of wave energy converter M4," in *Asian Wave and Tidal Energy Conference*, Taipei, Taiwan, 2018. [Online]. Available: <https://tethys-engineering.pnnl.gov/sites/default/files/publications/AWTEC2018-425.pdf>
- [17] C. Lee and J. N. Newman, "Wamit – user manual version 7.0," in *WAMIT Inc, Chestnut Hill, Massachusetts*, 2013.
- [18] W.E.Cummins, "The impulse response function and ship motions," 1962. [Online]. Available: <https://dome.mit.edu/handle/1721.3/49049>
- [19] J. Apsley, X. Zhang, M. Iacchetti, I. E. Damian, Z. Liao, G. Li, P. Stansby, G. Li, H. Wolgamot, C. Gaudin, A. Kurniawan, X. Zhang, Z. Lin, N. Fernando, C. Shearer, and B. Saunders, "Integrated hydrodynamic-electrical hardware model for wave energy conversion with m4 ocean demonstrator," *Proceedings of the European Wave and Tidal Energy Conference*, vol. 15, Sep. 2023. [Online]. Available: <https://submissions.ewtec.org/proc-ewtec/article/view/500>
- [20] X. Zhang, J. Apsley, and M. Iacchetti, "Computationally-efficient Modelling of Wave Energy Conversion Systems via Pseudo Steady-State PMSM Model," in *11th International Conference on Power Electronics - ECCE Asia, ICC, Jeju, Korea*, 2023.
- [21] A. Bodrov, "Performance of multi-drive systems," Ph.D. dissertation, The University of Manchester (United Kingdom), 2019.
- [22] G. Li and M. R. Belmont, "Model predictive control of sea wave energy converters—part i: A convex approach for the case of a single device," *Renewable Energy*, vol. 69, pp. 453–463, 2014.
- [23] Z. Liao, T. Sun, M. Al-Ani, L.-B. Jordan, G. Li, Z. Wang, M. Belmont, C. Edwards, and S. Zhan, "Modelling and control tank testing validation for attenuator type wave energy converter - part ii: Linear noncausal optimal control and deterministic sea wave prediction tank testing," *IEEE Transactions on Sustainable Energy*, pp. 1–10, 2023.
- [24] Z. Liao, P. Stansby, and G. Li, "A generic linear non-causal optimal control framework integrated with wave excitation force prediction for multi-mode wave energy converters with application to m4," *Applied Ocean Research*, vol. 97, p. 102056, 2020. [Online]. Available: <http://www.sciencedirect.com/science/article/pii/S0141118719305012>
- [25] A. Kurniawan, H. Wolgamot, C. Gaudin, C. Shearer, P. Stansby, and B. Saunders, "Numerical modelling in the development of the m4 prototype for Albany, western Australia," in *Proceedings of the ASME 2023 42nd International Conference on Ocean, Offshore and Arctic Engineering OMAE2023*, Melbourne, Australia, June 11–16, 2023.
- [26] T. Sun, Z. Liao, M. Al-Ani, L.-B. Jordan, G. Li, M. Belmont, C. Edwards, and S. Zhan, "Modelling and control tank testing validation for attenuator type wave energy converter—part iii: Model predictive control and robustness validation," *IEEE Transactions on Sustainable Energy*, pp. 1–10, 2023.